Accepted Manuscript

Pyridazinone-substituted benzenesulfonamides display potent inhibition of membrane-bound human carbonic anhydrase IX and promising antiproliferative activity against cancer cell lines

Mikhail Krasavin, Anton Shetnev, Sergey Baykov, Stanislav Kalinin, Alessio Nocentini, Vladimir Sharoyko, Giulio Poli, Tiziano Tuccinardi, Mikhail Korsakov, Tatiana B. Tennikova, Claudiu T. Supuran

PII: S0223-5234(19)30158-8

DOI: https://doi.org/10.1016/j.ejmech.2019.02.044

Reference: EJMECH 11136

To appear in: *European Journal of Medicinal Chemistry*

Received Date: 25 January 2019

Revised Date: 10 February 2019

Accepted Date: 12 February 2019

Please cite this article as: M. Krasavin, A. Shetnev, S. Baykov, S. Kalinin, A. Nocentini, V. Sharoyko, G. Poli, T. Tuccinardi, M. Korsakov, T.B. Tennikova, C.T. Supuran, Pyridazinone-substituted benzenesulfonamides display potent inhibition of membrane-bound human carbonic anhydrase IX and promising antiproliferative activity against cancer cell lines, *European Journal of Medicinal Chemistry* (2019), doi: https://doi.org/10.1016/j.ejmech.2019.02.044.

Pyridazinone-substituted benzenesulfonamides display potent inhibition of membrane-bound human carbonic anhydrase IX and promising antiproliferative activity against cancer cell lines

Mikhail Krasavin*, Anton Shetnev, Sergey Baykov, Stanislav Kalinin, Alessio Nocentini, Vladimir Sharoyko, Giulio Poli, Tiziano Tuccinardi, Mikhail Korsakov, Tatiana B. Tennikova, Claudiu T. Supuran*

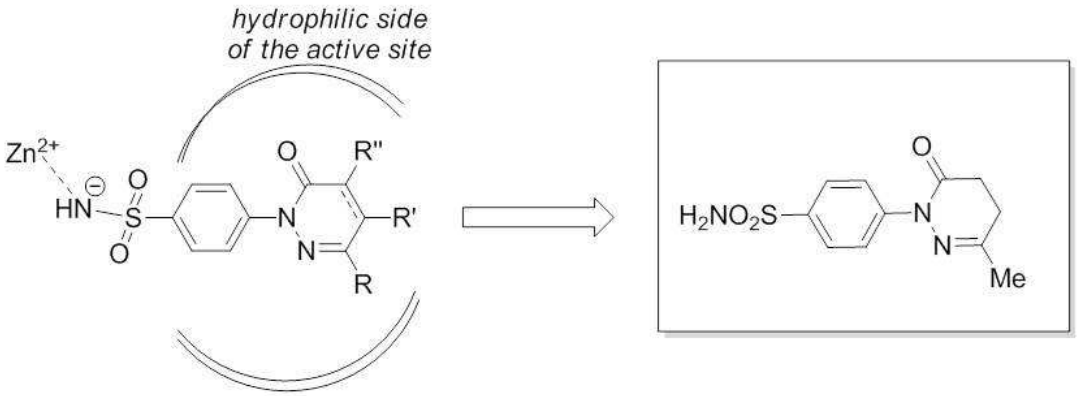

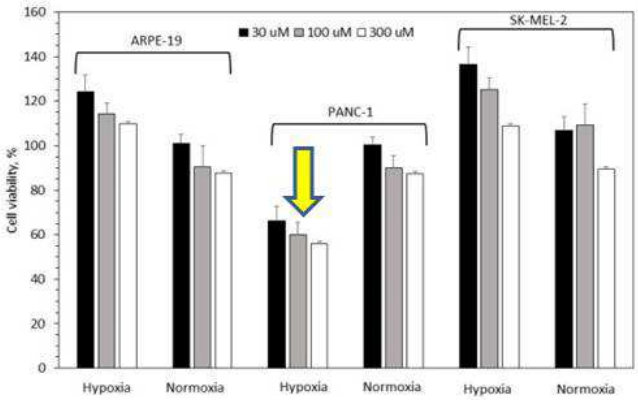

Ki (nM)

*h*CA I	88.2	*Cytosolic off-targets*
*h*CA II	0.68	
*h*CA IX	32.8	*Membrane-bound cancer targets*
*h*CA XII	31.0	

Pyridazinone-substituted benzenesulfonamides display potent inhibition of membrane-bound human carbonic anhydrase IX and promising antiproliferative activity against cancer cell lines

Mikhail Krasavin[a,*], Anton Shetnev[b], Sergey Baykov[a], Stanislav Kalinin[a], Alessio Nocentini[c], Vladimir Sharoyko[a], Giulio Poli[d], Tiziano Tuccinardi[d], Mikhail Korsakov[b], Tatiana B. Tennikova[a], Claudiu T. Supuran[c,*]

[a] Saint Petersburg State University, Saint Petersburg, 199034 Russian Federation

[b] The Ushinsky Yaroslavl State Pedagogical University, Yaroslavl 150000, Russian Federation

[c] Neurofarba Department, Universita degli Studi di Firenze, Florence, Italy

[d] Department of Pharmacy, University of Pisa, 56126 Pisa, Italy

* Corresponding authors. E-mail addresses: m.krasavin@spbu.ru (M. Krasavin), claudiu.supuran@unifi.it (C. T. Supuran)

ABSTRACT

An expanded set of pyridazine-containing benzene sulfonamides was investigated for inhibition of four human carbonic anhydrase isoforms, which revealed a pronounced inhibition trend toward *h*CA IX, a cancer-related, membrane-bound isoform of the enzyme. Comparison of antiproliferative effects of these compounds against cancer (PANC-1) and normal (ARPE-19) cells at 50 μM concentration narrowed the selection of compounds to the eight which displayed selective growth inhibition toward the cancer cells. More detailed investigation in concentration-dependent mode against normal (ARPE-19) and two cancer cell lines (PANC-1 and SK-MEL-2) identified two lead compounds one of which displayed a notable cytotoxicity toward pancreatic cancer cells while the other targeted the melanoma cells. These findings significantly expand the knowledge base concerning the hCA IX inhibitors whose inhibitory potency against a recombinant enzyme translates into selective anticancer activity under hypoxic conditions which are aimed to model the environment of a growing tumor.

Keywords: carbonic anhydrase; isoform-selective inhibitors; periphery groups; primary sulfonamides; subnanomolar inhibition; pyridazinone; phthalazinone, cancer cells; hypoxic environment; growth inhibition assay.

1. Introduction

The fundamental biochemical reaction of reversible hydration of carbon dioxide catalyzed by the human carbonic anhydrases (*h*CAs) [1] produces bicarbonate anion and a proton and is, therefore, an important regulatory mechanism for controlling the intra- and extracellular pH in various part of the human body. Among the 15 *h*CA isoforms (each of them having different cellular localization, catalytic activity and expression levels in normal vs. aberrantly functioning cells [2]), many are already validated as targets for drug intervention while novel links to various disease continue to be discovered [3]. Likewise, selective inhibition of pathogen CAs, not interfering with the host hCA machinery, presents an attractive new option for antibiotic development and is receiving increase attention. [4]. These new approaches to disease treatment require that small molecules intended to produce a certain therapeutic effect are isoform-selective and do not to affect the normal functioning of other isoforms, not involved in the disease. Today, however, all clinically used carbonic anhydrase inhibitors (such as diuretics [5] or drugs used to treat glaucoma-related intraocular hypertension [6]) are predominantly non-selective as *h*CA inhibitors (Fig. 1).

		K_i (nM)			
		*h*CA I	*h*CA II	*hCA* IX	*h*CA XII
acetazolamide	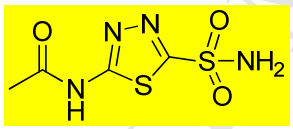	250	12	25	5.7
methazolamide	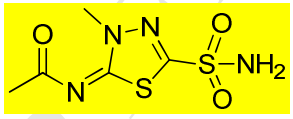	50	14	27	3.4
dorzolamide		50,000	9	52	3.5
brinzolamide	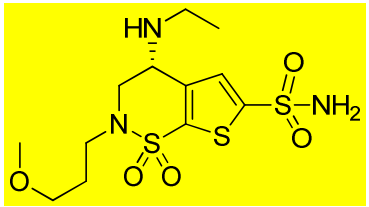	45,000	3	37	3.0

Fig. 1. Examples of clinically used, non-selective *h*CA inhibitors and their inhibition profile [7] against the panel of human carbonic anhydrases (*h*CAs) interrogated in this work.

That being said, the landscape of investigational isoform-selective carbonic anhydrase inhibitors (CAIs) has been widening. Noteworthy examples are isoxazole bis-sulfonamide inhibitor of

membrane-bound *h*CA IV (**1**) [8], dual inhibitor of cytosolic *h*CA II and VII based on 2-imidazoline scaffold (**2**) [9], selective biphenyl sulfonamide inhibitor of *h*CA XIV (**3**) [10], and ring-opened *N*-alkyl saccharin derivative (**4**) selective for tumor-associated, membrane-bound isoforms hCA IX and XII [11]. In the clinical phases of development, *h*CA IX-selective drug SLC-0111 has now successfully completed phase I clinical trials for tumors overexpressing CA IX [12] and is scheduled to enter phase II clinical trials in the near future. E7070 (indisulam) was developed as novel antineoplastic therapy by Eisai Co., Ltd. It entered clinical development in 2005 and is currently in phase II clinical trials in the US and Europe [13]. Notably, from the inhibition profile of SLC-0111 and, particularly, of E7070 it is evident that selectivity over the cytosolic off-target *h*CA II isoform is not a pre-requisite to achieving clinical efficacy in cancer treatment (Fig. 2).

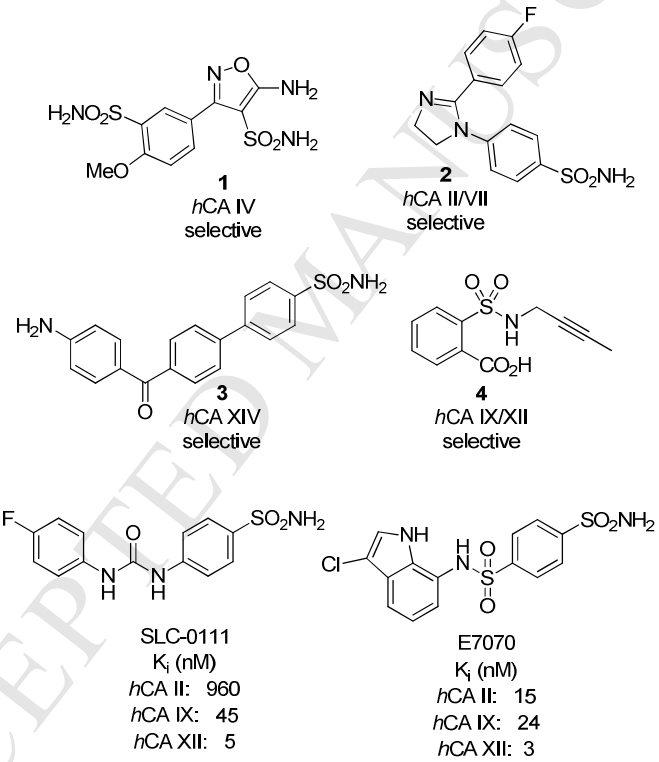

Fig. 2. Examples of recently reported isoform-selective hCA inhibitors (**1**-**4**) and structures of the most advanced *h*CA IX/XII-selective CAIs (SLC-0111 and E7070) currently in clinical trials for cancer.

A metastatic tumor can survive and grow in the stressful hypoxic and acidic extracellular environment surrounding it by overexpressing the membrane-bound *h*CA IX and *h*CA XII isoforms [14] while inhibition of the latter can potentially retard the tumor growth and reduce its size [15]. Today, mounting evidence has been gathered for tumors able to develop resistance to various targeted small-molecule therapies [16]. In contrast, inhibition of *h*CA IX and *h*CA XII overexpressed on the surface of tumor cells targets a fundamental mechanism of their survival, at

the level of evolutionary primordial animatic machinery. Hence, the likelihood of resistance emerging to drugs acting via this mechanism is considered low, which makes the latter an attractive approach for small molecule intervention [17].

The majority of known CAIs are primary aromatic and heteroaromatic sulfonamides in which the sulfonamide group acts as a metal binding motif and ensures affinity to the enzyme by coordinating to its prosthetic Zn^{2+} ion [18], a binding mode universal for all *h*CA isoforms. It is the molecular periphery of the inhibitor that can provide an additional binding to a particular isoform and thus be the principal source of isoform-selective inhibition [19]. Thus exploration of various periphery motifs for the pharmacophoric sulfonamide part of the prospective inhibitor (via random screening or based on *in silico* modeling [20]) is especially significant for the ongoing quest for selectively targeted CAIs.

In the course of exploring various substituted heterocyclic appendages for the CAI pharmacophoric arene sulfonamide moiety (such as 1,3-oxazole [21], isoxazole [8], imidazoline [9, 20], pyrazole [22] and 1,2,4-oxadiazole [23]), it came to our attention that pyridazinone-substituted benzenesulfonamides **5** had been discovered and studied as potent inhibitors of cytosolic *h*CA I and *h*CA II isoforms (as exemplified by compound **5a**) [24]. Such a potent inhibitory profile is perhaps unsurprising considering the almost ideal positioning of the polar (pyridazinone carbonyl) and lipophilic (aromatic group) portions of the compound's periphery for cooperative contacts with the respective, distinctly delineated in hydrophobic character, portions of the enzyme's active site [19]. Considering this clear predisposition of representatives of this chemotype to act as CAIs in general, we thought it important to prepare an expanded set of analogs of pyridazinone-containing compounds and evaluate its inhibitory properties toward the cancer-related, membrane-bound isoforms *h*CA IX and *h*CA XII. In addition to substituted pyridazinone analogs **6** of the previously reported series [24], we aimed to explore their non-aromatic analogs **7** as well as their differently substituted analogs **8** and benzene-fused series **9**. In all cases we expected the carbonyl group of the pyridazinone nucleus to effectively address the hydrophilic side of the enzyme's active site while the peripheral substituents would be increasing the binding efficiency by interacting with the hydrophobic portion of the same (Fig. 3). Our ultimate goal was to identify compounds that display the clear propensity to inhibit the *h*CA IX and/or *h*CA XII cell surface-bound isoforms (with or without inhibition of the cytosolic off-targets hCA I and hCA II which are less important in the context of this study) and further determine their potential to target cancer cells under hypoxic conditions (i. e. in the environment where catalytic activity of these two isoforms becomes crucial for the cells' survival and growth, *vide supra*). Herein, we present the results of these studies.

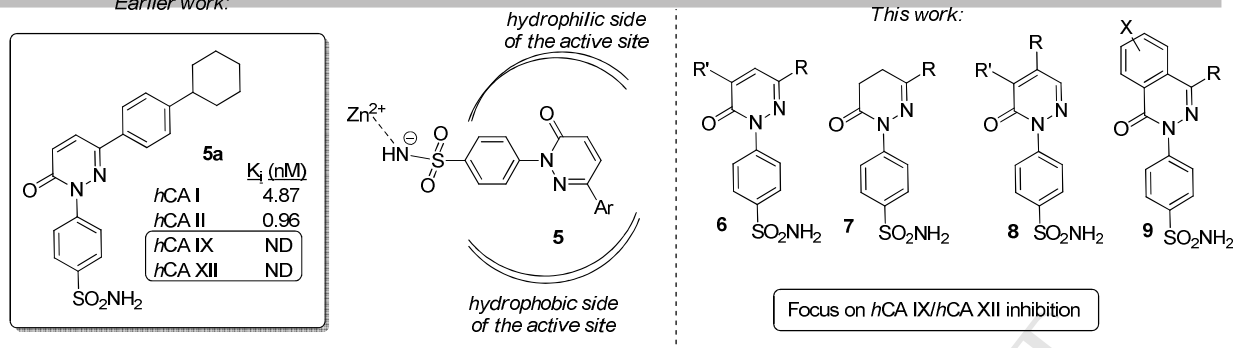

Fig. 3. Earlier reported pyridazinone-substituted benzenesulfonamides **5** (their design rationale and CAI profile for a representative compound (**5a**)) and for series of analogs explored in this work with respect to their *h*CA IX/*h*CA XII inhibition potential.

2. Results and discussion

2.1. Chemistry

A series of aromatic methyl ketones **10** were condensed with glyoxalic or pyruvic acid in aqueous basic solution as described previously [25]. The intermediate compounds **11**, without isolation, were treated with an ethanolic solution of 4-hydrazinobenzenesulfonamide hydrochloride salt (**12**) at reflux. This led to the conversion of the hydrazine component to the free base form and subsequent condensation to form the pyridazinone ring and gave the target compounds **6a-d** in moderate to good yields (Scheme 1) [25].

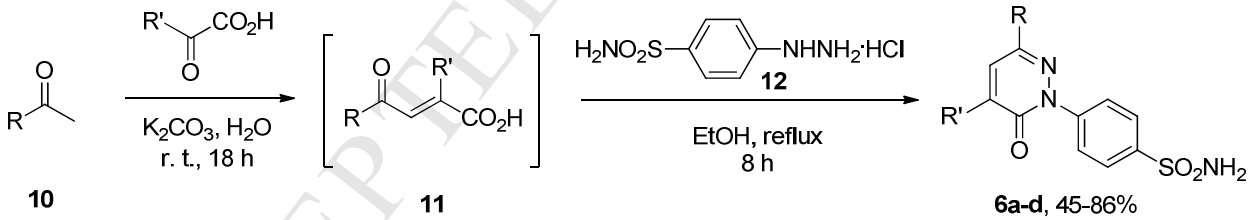

Scheme 1. Synthesis of compounds **6a-d** investigated in this work.

Compounds **7a-d** belonging to the 5,6-dihydropyridazinone series were generated by similar cyclocondensation between **12** and a series of commercially available γ-ketocarboxylic acids **13**, which provided the target compounds in good to excellent yields (Scheme 2) [26].

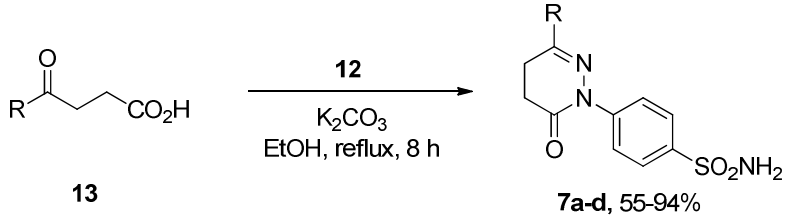

Scheme 2. Synthesis of compounds **7a-d** investigated in this work.

Similar condensation between **12** and mucochloric acid (**14**) yielded compound **8a** in excellent yield. Both chlorine atoms in **8a** were removed by catalytic hydrogenation over 10% Pd on carbon to give compound **8b** in 79% yield [27]. At the same time, according to the literature data [28], chlorine atom in position 5 of pyridazinone ring is more labile toward aromatic nucleophilic substitution and thus it was replaced with a range of aliphatic amines in refluxing ethanolic solution in the presence of triethylamine [29] to give compounds **8c-i** in good to excellent yields. Catalytic hydrogenation of a selected set of the latter provided compounds **8j-l** in high yield (Scheme 3).

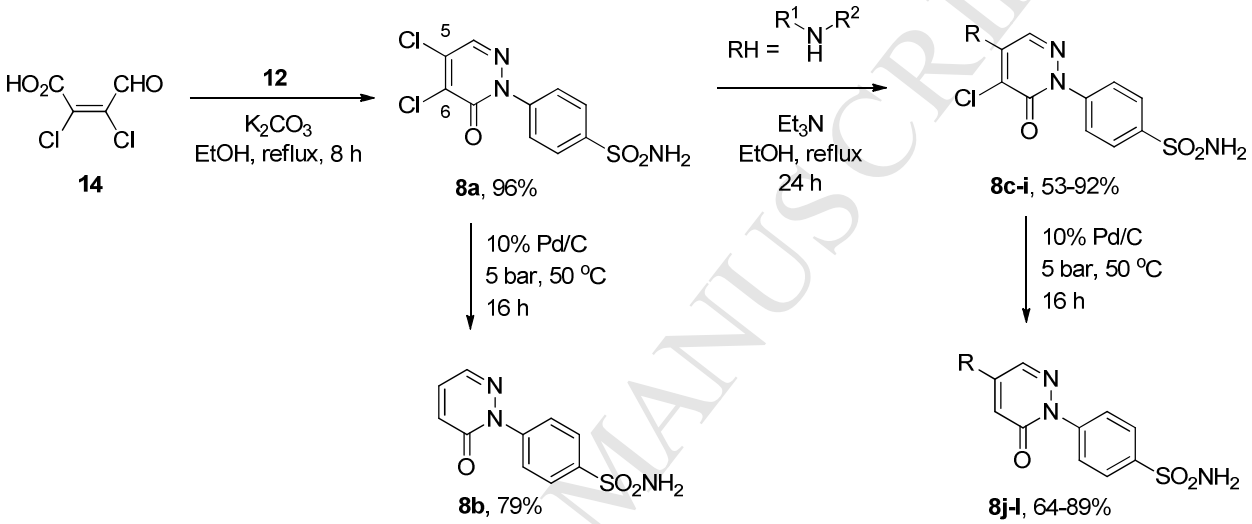

Scheme 3. Synthesis of compounds **8a-l** investigated in this work.

Finally, condensation of **12** with a small set of *o*-acylbenzoic acids **15** gave phthalazinone compounds **9a-c** in excellent yield (Scheme 4).

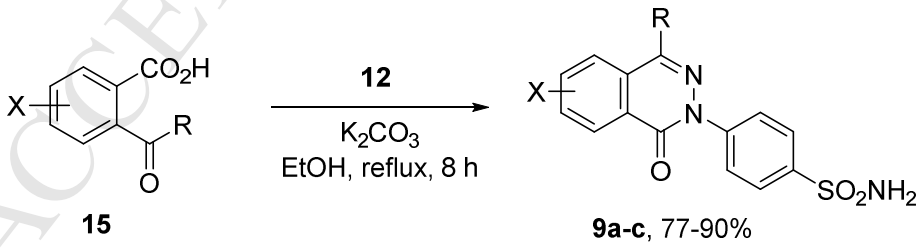

Scheme 4. Synthesis of compounds **9a-c** investigated in this work.

2.2. Biochemical testing for CA inhibition

The twenty-three primary sulfonamide compounds **6a-d**, **7a-d**, **8a-l** and **9a-c** synthesized as detailed above, were tested in CO_2 hydration stopped-flow biochemical assay (see Experimental

section) against two cytosolic (*h*CA I and II) and two membrane-bound, cancer-related *h*CA IX and XII isoforms to produce the inhibition data (K_i) summarized in Table 1.

Table 1. Inhibitory profile of compounds **6a-d**, **7a-d**, **8a-k** and **9a-c** against *h*CA I, II, IX and XII.[a]

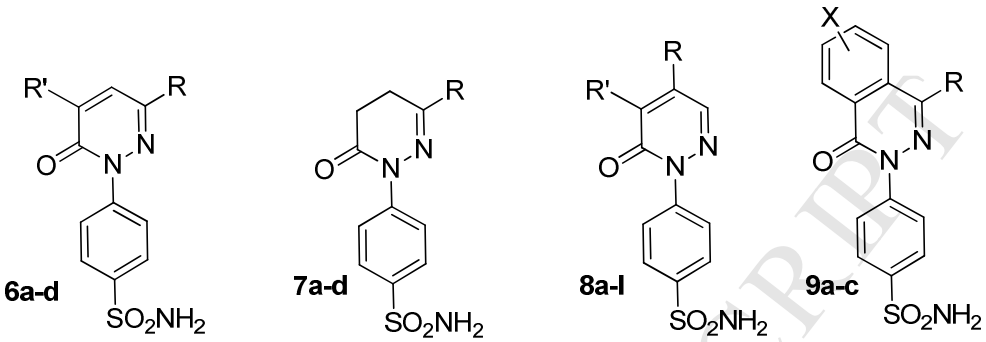

Compound	R	R′	X	K_i (nM)			
				*h*CA I	*h*CA II	*h*CA IX	*h*CA XII
6a	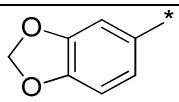	H	--	99.0	1.40	28.2	63.70
6b	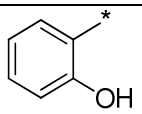	H	--	84.1	0.62	0.46	9.30
6c	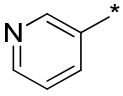	Me	--	100.5	2.90	2.30	8.80
6d	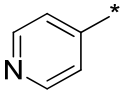	H	--	227.4	4.8	50.8	8.70
7a	Me	--	--	88.2	0.68	32.8	31.0
7b	Ph	--	--	186.6	0.26	4.80	22.5
7c	4-$MeOC_6H_3$	--	--	92.7	0.08	2.40	9.90
7d	3,4-diClC_6H_3	--	--	5962	74.1	6.00	67.1
8a	Cl	Cl	--	482.1	2.30	8.70	9.90
8b	H	H	--	320.4	8.20	9.00	81.2
8c	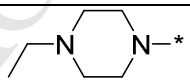	Cl	--	485.3	0.29	0.70	7.20
8d	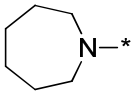	Cl	--	97.4	0.06	0.49	8.40
8e	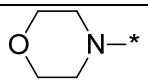	Cl	--	89.0	0.07	0.58	36.0
8f	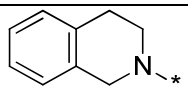	Cl	--	738.4	60.5	89.6	85.5
8g	BnNH	Cl	--	95.1	0.09	0.67	9.40

8h	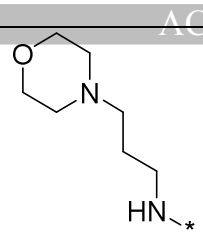	Cl	--	481.5	0.67	2.80	10.1
8i	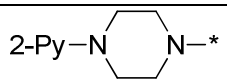	Cl	--	676.1	46.6	89.5	105.1
8j	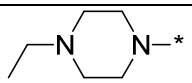	H	--	311.3	4.30	41.3	25.3
8k	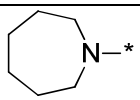	H	--	88.2	0.08	0.56	6.30
8l	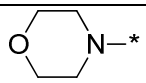	H	--	292.3	0.55	2.10	9.80
9a	--	--	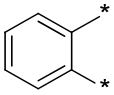	72.3	0.23	0.32	50.6
9b	--	--	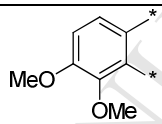	90.7	3.50	8.90	66.4
9c	Me	--	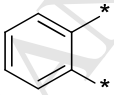	89.7	0.03	0.24	9.00

[a] Mean K_i values from 3 different stopped-flow assays (errors were in the range of ±5-10% of the reported values).

From a brief examination of the data presented in Table 1, it becomes evident that in general, the compounds prepared and investigated in this work retained subnanomolar to low nanomolar inhibitory potency against cytosolic *h*CA II isoform while the potency toward *h*CA I (also a cytosolic form) decrease dramatically in comparison to the earlier reported data (cf. compound **5a**). At the same time, the inhibitory potency toward cancer-related *h*CA IX was established to reach into the subnanomolar range, thereby making this diverse series of compounds worthy further investigation as antiproliferative agents for cancel cells under hypoxic conditions. Particularly encouraging is a concomitant inhibition of *h*CA XII isoform, albeit with surprisingly flat SAR (i.e., the single- to double-digit nanomolar inhibition of this isoform appears insensitive to variations in the inhibitor structure). It should be noted that inhibition of *h*CA II, in general, does not present a significant obstacle to antitumor efficacy (as evidenced by the advanced status of compound E7070 (indisulam), also a dual *h*CA II/IX inhibitor, currently in clinical trial for cancer [13]). Moreover, considering the vastly different cellular localization of these two isoforms, the de facto selectivity will be governed in the end by the potentially higher extracellular vs. intracellular concentration of the inhibitor [30].

Notable SAR facts that surface from the data presented in Table 1, include the relative insensitivity of the inhibitory profile to the substitutions around the flat pyridazinone core as far as large substituents in position 4 are concerned. Indeed, the profile of compounds **6a-d** is nearly identical to that of bis-chloro compound **8a** and unsubstituted compound **8b**. At the same time, in the non-flat, 5,6-dihydropyridone series, *h*CA II potency appears quite sensitive to the nature of the aromatic group (cf. compounds **7c** and **7d** displaying a ~1000-fold drop in inhibitory activity). Similarly sensitive to the substitution pattern appears the phthalazinone series where introduction of a methyl group in compound **9c** improved the *h*CA II potency 10-fold compared to compounds **9a**. However, the dimethoxy substitution in compound **9b** appears to be detrimental to both *h*CA II and *h*CA IX inhibition. In the amino-substituted pyridazinone series, only tetrahydroisoquinoline substitution in **8f** appears to lead to poorer inhibition (compared, for instance, to its 'disconnected' analog **8g**) of both *h*CA II and *h*CA IX. The inhibitory profile of the chlorinated amino-substituted compounds looks similar to that of their des-chloro counterparts, except for the pair **8c**/**8j** where removal of the chlorine atom lead to a 10-fold drop in *h*CA II and *h*CA IX potency.

2.3. Docking studies

In order to provide rational interpretations of the SAR data derived from the experimental results, representative compounds belonging from the different series of synthesized derivatives were studies through a molecular modeling analysis comprising a robust docking procedure followed by energy minimization in explicit water environment (see Experimental section for details). The phthalazinone derivatives **9a** and **9c**, which showed subnanomolar potency against *h*CA II and *h*CA IX, were docked into the catalytic site of the two enzymes with the aim of evaluating their potential binding mode. Compound **9a** was predicted to chelate the prosthetic zinc ion of *h*CA II through the sulfonamide group, which also interacts with T198 forming H-bonds with both the backbone nitrogen and the hydroxyl group of the residue (Fig. 4A). The phenylene linker of the ligand shows van der Waals interactions with H94 and Q92 from one side and takes hydrophobic contacts with V121, L140 and especially L197 from the other side. Finally, the phthalazinone moiety is placed into the narrow space delimited by I91, Q92, V121 and F130, forming a strong π-π stacking with F130 and an H-bond with the side chain of Q92 established through its carbonyl oxygen. The binding mode generated for **9a** into *h*CA IX is very similar to the disposition predicted into *h*CA II, in agreement with the comparable activity of the ligand toward the two enzyme isoforms (Fig. 4B). In fact, compound **9a** forms the same pattern of H-bonds and lipophilic interactions with the homolog residues of *h*CA IX, with the only exception of the π-π stacking interaction that is absent due to the presence of V262 in place of

the non-conserved residue F130 (*h*CA II). However, the ligand is still able to form strong van der Waals interactions with the flat hydrophobic wall of *h*CA IX constituted by L223, V262 and L266.

The increase in *h*CA II inhibitory activity obtained by the introduction of a methyl group in compound **9c** seems to be due to improved hydrophobic interactions and a stabilization of the binding pose, compared to **9a**. In fact, the methyl group of **9c**, well fits a small hydrophobic pocket delimited by F130, V134, I197 and P201, formed by the protrusion of F130 side chain towards the entrance of the binding site. The interaction into this pocket contributes to lock the ligand into its binding disposition, besides allowing additional lipophilic contacts with the pocket residues (Fig. 4C). Interestingly, compound **9c** maintains the H-bond with Q92 and a T-shaped stacking interaction with F130. The observation that no potency improvement against *h*CA IX is obtained for **9c** with respect to **9a** is in agreement with the absence of the small hydrophobic pocket within *h*CA IX binding site. On the contrary, the *h*CA II potency drop obtained by the introduction of the two methoxy groups in compound **9b** can be rationalized by considering the steric bulk of the two substituents, which would prevent the ligand to be placed into the narrow space between Q92 and F130. In fact, compound **9b** is predicted to dispose the phthalazinone core perpendicularly with respect to the binding mode of **9a**, in order to avoid steric hindrance with the surrounding residues (Fig. 4D). However, this is paid with the loss of the H-bond with Q92, which is consistent with the reduced activity of the ligand. Similar considerations can be also valid for justifying the activity of the ligand against *h*CA IX, which is comparable to that shown against *h*CA II.

Among the amino-substituted pyridazinone derivatives, compound **8c** showed subnanomolar potency against both *h*CA II and *h*CA IX, while its des-chloro analogue **8j** was found to have reduced activity. The predicted binding mode of the two compounds into *h*CA II is similar and consistent with the binding disposition hypothesized for compound **9a** (Fig. 4A). In fact, besides the sulfonamide groups, also the phenylene linker and the phthalazinone ring of **8c** and **8j** present an orientation comparable with that observed for **9a**, forming a similar pattern of interactions with the surrounding protein residues, included the H-bond with the side chain of Q92 (Fig. 5). However, the π-π stacking with F130 is not shown due to the absence of the fused phenyl ring in **8c** and **8j**, but the positively charged piperazine groups of the two ligands are able to form a water-bridged interaction with E69. The positive effect on ligand potency determined by the chlorine atom could be due to the additional hydrophobic contacts and a better shape complementarity with the protein observed in compound **8c** with respect to **8j**. In fact, the chlorine atom can form extensive lipophilic interactions with I91, Q92, V121 and F130 that can

also compensate for the lack of π-π stacking with F130 and stabilize the ligand disposition into the protein catalytic site, thus justifying the higher potency of **8c** compared to **8j**. The reduced activity of both ligands against *h*CA IX can be ascribed to the fact that E69 of *h*CA II is a non-conserved residue replaced by a threonine in *h*CA IX; therefore, the two ligands cannot form the water-bridged interaction with E69. However, while **8c** shows only a slight (2.5-fold) decrease in potency, compound **8j** presents a 10-fold lower activity on *h*CA IX compared to *h*CA II: this data is consistent with the binding mode proposed for the two derivatives, considering the less direct interaction with E69 predicted for **8c** (mediated by two water molecules instead of one as in **8j**) and the presence of the chlorine atom, which can reduce the impact of the missing interaction with E69, compared to **8j**.

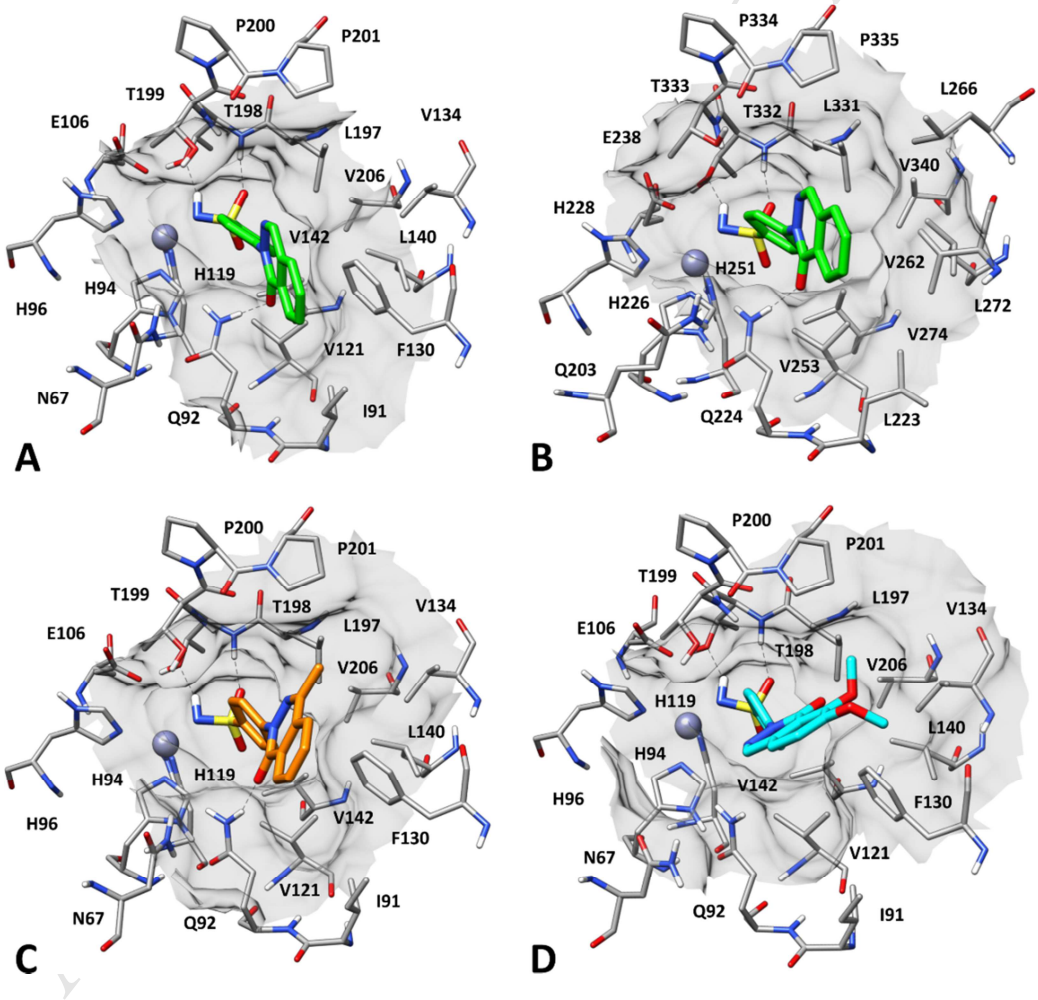

Fig. 4. Predicted binding mode of compound **9a** into *h*CA II (A) and *h*CA IX (B); predicted binding mode of compound **9c** (C) and **9b** (D) into *h*CA II. Ligand-protein H-bonds are shown as black dashed lines, the protein surface in the proximity of the ligands is shown in grey.

Finally, a different water-bridged interaction could contribute to the different *h*CA II inhibitory potency observed for the non-flat 5,6-dihydropyridone derivatives **7c** and **7d**. Compound **7c**, which showed picomolar potency against *h*CA II, was predicted to assume a binding mode in

line with those calculated for the other *h*CAIs herein analyzed. Interestingly, despite the distortion introduced in the core ring due to the lack of aromaticity, the ligand is still able to form an H-bond with Q92 and extensive hydrophobic interactions with F130. Moreover, although the methoxyphenyl group of the ligand is highly solvent exposed, the water-mediated H-bond with W5 can counterbalance the unfavorable desolvation effect and positively contribute to the ligand potency. On the contrary, the double chlorinated analogue **7d** is not able to form a similar interaction and it was predicted to orient its dichlorophenyl ring differently, in order to prevent any steric hindrance with W5 and to maximize the lipophilic interactions with both this and other residues such as H64 and N67. However, this different disposition also prevents the formation of the H-bond with Q92, thus contributing to explain the considerable reduction in *h*CA II potency of **7d** with respect to **7c** (Fig. 6).

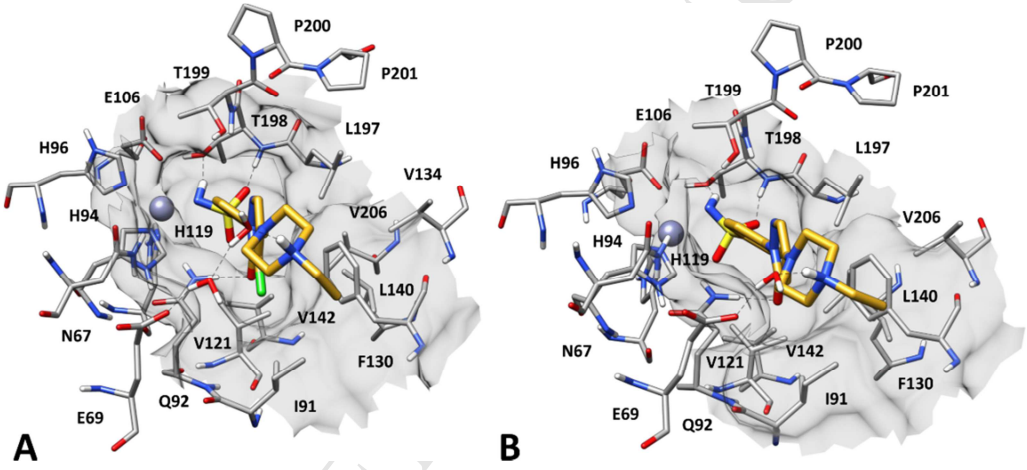

Fig. 5. Predicted binding mode of compound **8c** (A) and **8j** (B) into *h*CA II (A). Ligand-protein H-bonds are shown as black dashed lines, the protein surface in the proximity of the ligands is shown in grey.

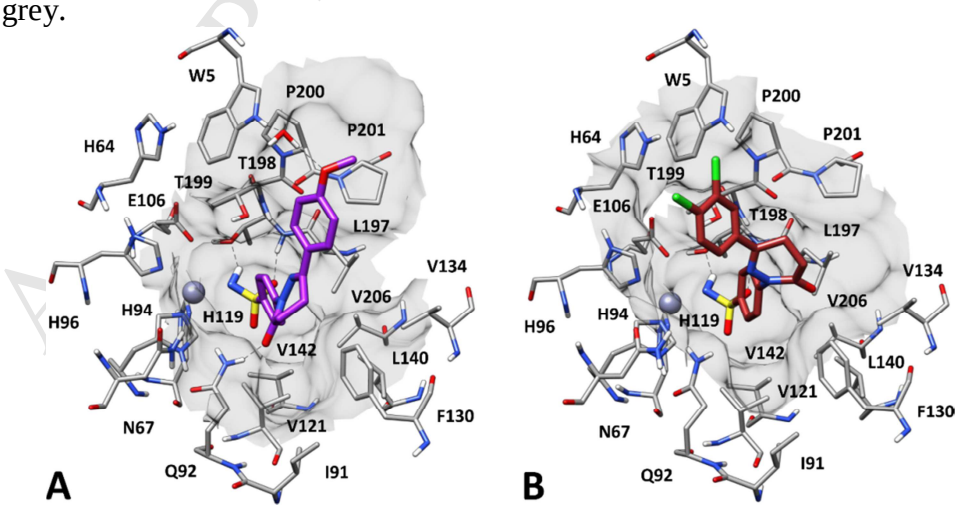

Fig. 6. Predicted binding mode of compound **7c** (A) and **7d** (B) into *h*CA II. Ligand-protein H-bonds are shown as black dashed lines, the protein surface in the proximity of the ligands is shown in grey.

2.4. Antiproliferative activity against normal and cancer cell lines

The potent inhibition of membrane-bound, cancer-related enzyme *h*CA IX by virtually all compounds **6a-d**, **7a-d**, **8a-l** and **9a-c** (some of them reaching into the subnanomolar potency range), on top of fairly promising inhibition profile with respect to *h*CA XII, clearly warranted their further investigation for antiproliferative effects in cancer cells. As we already mentioned the absence of selectivity between these isoforms and also against *h*CA II should not be perceived as a substantial disadvantage, considering the fact the vastly different cellular localization of these targets and, as a result, the potential for gaining selectivity by suppressing cell membrane permeability in the course of subsequent lead optimization [30]. While evaluation of the antiproliferative profile for cancer cells in comparison to normal cells should be performed under normoxic as well as hypoxic conditions, sulfonamide CAs are known to be more likely to exert their cytotoxicity profile under hypoxic conditions, i. e. those that closely reproduce the environment of a growing solid tumor, particularly with respect to pH disbalance and overexpression of *h*CA IX and *h*CA XII isoforms [31].

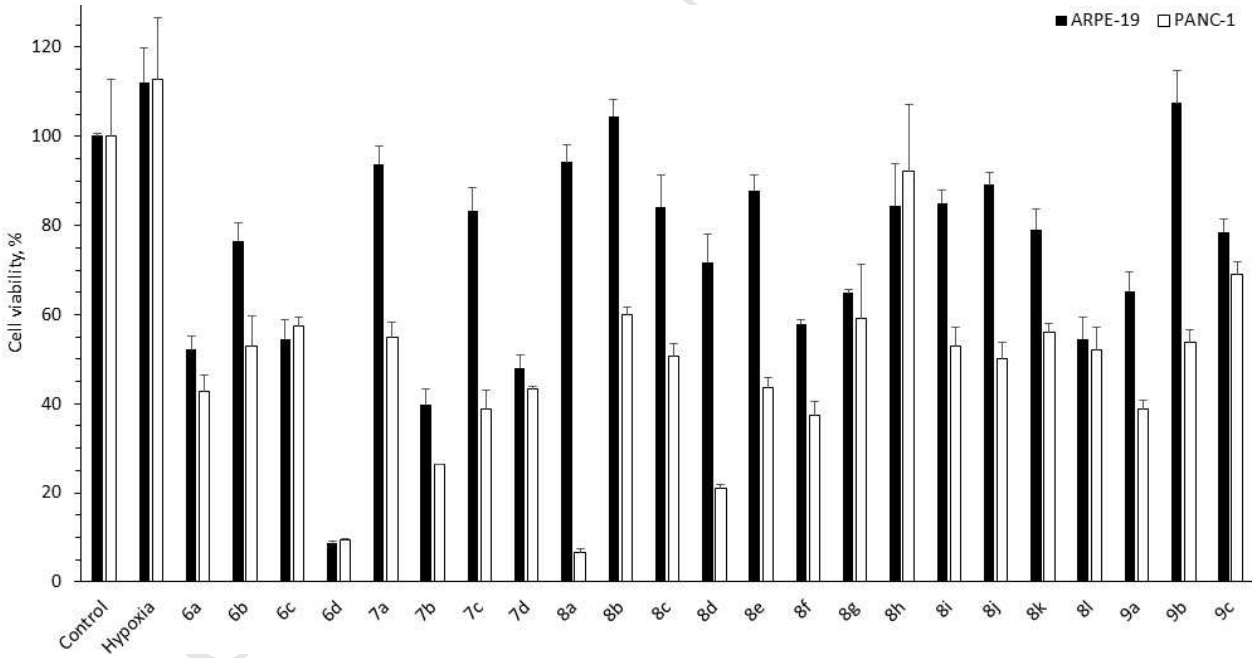

Fig. 7. Cell viability MTT assay results for compounds **6a-d**, **7a-d**, **8a-l** and **9a-c** (50 μM) against APRE-19 and PANC-1 cell lines (values are expressed as the mean ± SEM of three experiments: (∗) $P < 0.05$ and (∗∗) $P < 0.01$ in comparison to control (0 μM).

Compounds **6a-d**, **7a-d**, **8a-l** and **9a-c** were screened at 50 μM concentration for their ability to affect the cell culture viability of non-cancerous human retinal pigment epithelial cell line ARPE-19 [32] as well as pancreas ductal adenocarcinoma cell line PANC-1 [33]. The initial testing was performed relative to control (0 μM of the test compounds) under chemically induced ($CoCl_2$) hypoxia [34]. As it is evident from the screening results presented in Fig. 7, cobalt(II) chloride itself did not affect the number of cells in the culture. Compound 6d, for some

reason, displayed a pronounced cytotoxicity toward the normal as well as cancer cells and thus was excluded from further consideration. However, a number of compounds (particularly, eight compounds **7a**, **7c**, **8a-e** and **8j**) proved to be >30% more cytotoxic towards PANC-1 vs. ARPE-19 cell line under the chemically induced hypoxia conditions and were thus perceived as leads worthy further characterization.

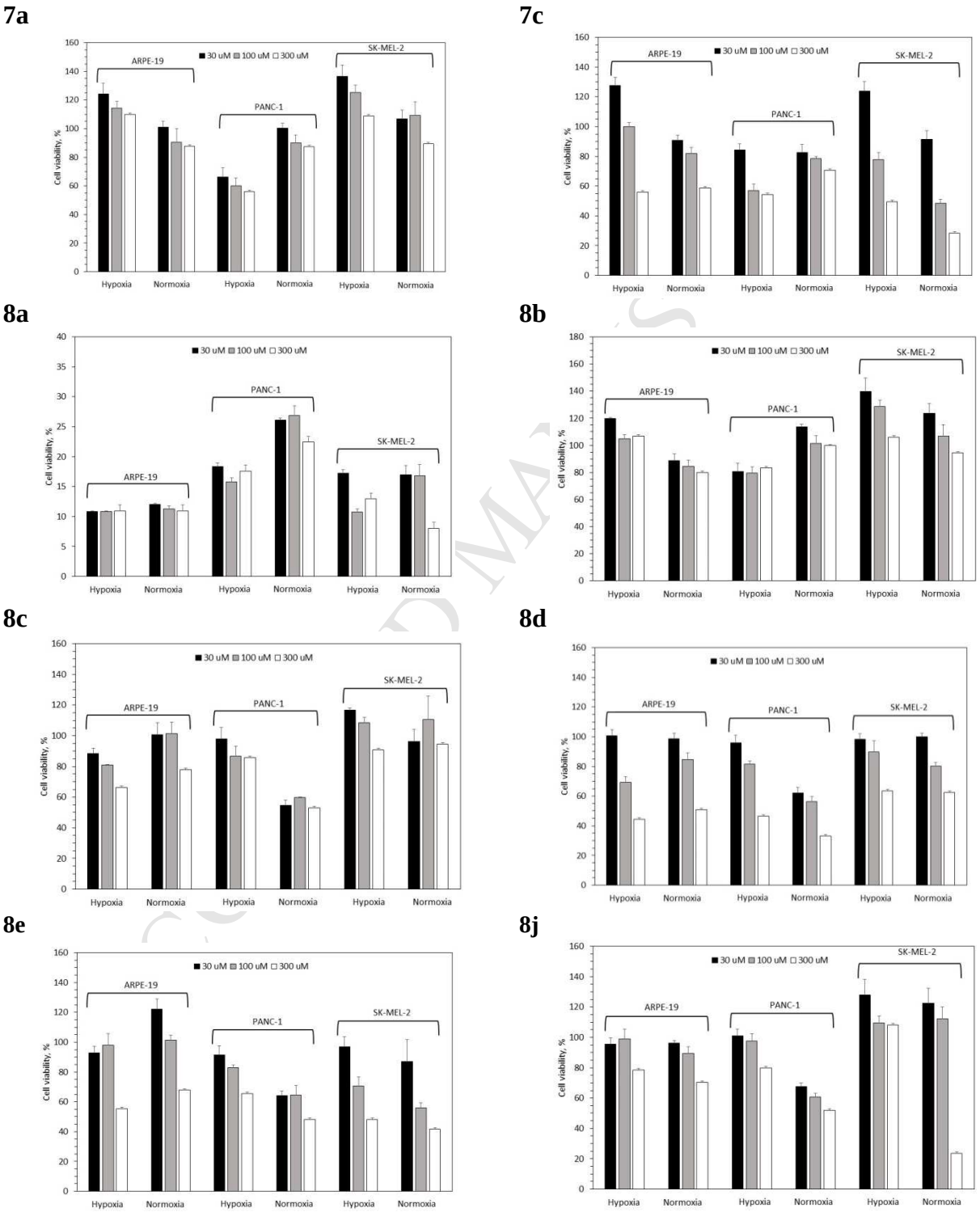

Fig. 8. Cell viability MTT assay results for compounds **7a**, **7c**, **8a-e** and **8j** (30 μM, 100 μM and 300 μM) against APRE-19, PANC-1 and MEL cell lines (values are expressed as the mean ± SEM of three experiments: (∗) $P < 0.05$ and (∗∗) $P < 0.01$ in comparison to control (0 μM, not shown).

These nine frontrunner compounds were tested in the MTT cell viability assay at three different concentrations (30 μM, 100 μM and 300 μM) against normal (ARPE-19) as well as two cancer cell lines (PANC-1 and also melanoma SK-MEL-2 [35] cell line), this time grown under normoxic as well as chemically induced hypoxic conditions. The antiproliferative profiles displayed by compounds **7a**, **7c**, **8a-e** and **8j** under this testing scheme are shown in Fig. 8.

Compound **8a** displayed a pronounced, non-selective cytotoxicity toward normal as well as both cancer cell lines. This behavior is likely a consequence of the compound's reactivity toward nucleophilic moieties which results in non-specific covalent modification of biomolecules. Similarly, compounds **7c** and **8d** displayed a dose-dependent cytotoxicity against ARPE-19 cells and thus were not considered further. Compounds **8b** and **8c** displayed no particular cytotoxicity neither to normal nor to cancerous cells, even at high concentration. Only at 300 μM concentration, compound **8j** appears selectively cytotoxic to melanoma cells. However, the main result of these comprehensive experiments, is that compound **8e** can be viewed as a promising cytotoxic agent for melanoma cells (under either hypoxic or normoxic conditions where it dose-dependently inhibited the growth of cancer cells but not normal cells) while compound **7a** was selectively cytotoxic to pancreatic cancer cell under hypoxic conditions. It is noteworthy that these agents belong to different structural classes and could be identified only via the 'screening funnel' scheme implemented in this work. It should be duly noted that in general, modeling of antitumor effects of *h*CA IX inhibitors by antiproliferative effects against a disperse cell culture, even grown under hypoxic conditions, is exceedingly difficult and requires cell viability screening at relatively high compound concentrations [31]. As the result, potent inhibition of *h*CA IX determined in a biochemical assay may not translate directly into similarly promising antiproliferative activity in vitro. This mandates that advanced candidates possessing promising antiproliferative profiles are selected from *h*CA IX based on preliminary cell viability testing and not only based on best K_i values.

3. Conclusion

By preparing and investigating an extended set of pyridazine-containing benzene sulfonamides, we established a pronounced propensity of this class of compounds to inhibit cancer-related, membrane bound isoform IX of human carbonic anhydrase (*h*CA IX), an observation that had not been made in the previous studies due to a limited number of isoforms included in the testing panel. This discovery prompted us to investigate the effects of these compounds on cancerous *vs.* normal cells under chemically induced hypoxia (i. e. the conditions rendering the catalytic

activity of *h*CA IX crucial survival mechanism of cancer cells. To our delight, eight compounds displayed a noticeable window between cytotoxicity against the normal (ARPE-19) and cancer (PANC-1) cells which warranted their further investigation. Testing these compounds at three different concentrations (30 μM, 100 μM and 300 μM) against ARPE-19 cells in comparison with PANC-1 and SK-MEL-2 cells revealed that one of the compounds (**7a**) displayed pronounced cytotoxicity toward pancreatic cancer cells while the other (**8e**) clearly targeted melanoma cells. The observed structure-activity relationships were analyzed by docking the key cornerstone compounds into the crystal structure of different isoforms, which allowed rationalizing the observed SAR trends. Altogether, these findings significantly expand the range of known *h*CA IX inhibitors whose biochemical activity translates (albeit indirectly) into the selective antiproliferative activity against cancer cells under hypoxic conditions that model the environment of a growing tumor.

4. Experimental section

4.1. General experimental

All and reagents and solvents were obtained from commercial sources and used without purification. All reactions implemented in an open flask without any protection from CO_2 and H_2O. Reactions were monitored by analytical thin layer chromatography (TLC) Macherey-Nagel, TLC plates Polygram® Sil G/UV254. Visualization of the developed chromatograms was performed by fluorescence quenching at 254 nm. ^{1}H and ^{13}C NMR spectra were measured on Bruker AVANCE DPX 400 (400 MHz for ^{1}H and 100 MHz for ^{13}C respectively). All chemical shifts (δ ppm) are given in parts per million (ppm) with reference to solvent residues in DMSO-d6-*d6* (2.50 for proton and 39.52 for carbon) and coupling constant (*J)* are reported in hertz (Hz). Multiplicities are abbreviated as follows: s = singlet, d = doublet, t = triplet, q = quartet, m = multiplet, br = broad. Melting points were determined on Electrothermal IA 9300 series Digital Melting Point Apparatus. Mass spectra were recorded on microTOF spectrometers (ESI ionization). Analytical HPLC was carried out on Shimadzu LC-20AP chromatograph equipped with spectrophotometric detector and Supelco Discovery C18, 5μm, 15cm×3mm column. Mobile phase: (A) 0.1% TFA in water – (B) 0.1% TFA in acetonitrile; gradient: 5–95% B (0 – 15min), 95% B (15 – 20min); flow rate 1 mL/min, temperature – 40 °C, detection UV at 214 and 254 nm. Injection volume 20μl. All compounds tested in biology assays were judged to be at least 95% pure by analytical HPLC.

4.2. Synthetic organic chemistry

General Procedure (GP1) for the synthesis of compounds 6a-d, 7a-d, 8a, 9a-c

A mixture of appropriate 1,4 - dicarbonyl compound **11, 13, 14 or 15** (0.001 mol) and 4-hydrazinobenzenesulfonamide hydrochloride **12** (0.001 mol) in ethanol (10–40 mL) was refluxed for 8-24 h. The reaction mixture was evaporated to give a crude solid. Crude product was stirred with 5-10 % sodium bicarbonate solution (25 mL) for 1h. It was filtered, washed with 2% acetic acid and then with water. It was dried and crystallized from ethanol to give (**6a-d, 7a-d, 8a, 9a-c**).

4-(3-(Benzo[d][1,3]dioxol-5-yl)-6-oxopyridazin-1(6H)-yl)benzenesulfonamide (**6a**)

Yield 174 mg (47%). Beige solid, m.p. 281-281,5°C, ^{1}H NMR (400 MHz, DMSO-d_6) δ ppm 8.12 (d, *J*= 9.8 Hz, 1H), 7.95 (q, *J*= 8.7 Hz, 4H), 7.54 – 7.43 (m, 4H), 7.18 (d, *J*= 9.8 Hz, 1H), 7.04 (d, *J*= 8.1 Hz, 1H), 6.11 (s, 2H). ^{13}C NMR (101 MHz, DMSO-d_6) δ ppm 158.95, 149.20, 148.59, 144.76, 144.46, 143.60, 131.77, 131.58, 128.65, 126.64, 126.41, 121.23, 109.01, 106.61, 102.09. HRMS (ESI, *m/z*): calculated for $C_{17}H_{13}N_3O_5S$ $[M+H]^+$ 372.0649; found 372.0643.

4-(3-(2-Hydroxyphenyl)-6-oxopyridazin-1(6H)-yl)benzenesulfonamide (**6b**)

Yield 165 mg (48 %). White solid, m.p. 269-270 °C. ^{1}H NMR (400 MHz, DMSO-d_6) δ ppm 10.38 (s, 1H), 8.01 (d, *J*= 9.8 Hz, 1H), 7.97 (d, *J*= 8.6 Hz, 2H), 7.91 (d, *J*= 8.6 Hz, 2H), 7.58 (d, *J*= 7.6 Hz, 1H), 7.56 - 7.33 (br. s, 2H), 7.31 (t, *J*= 7.7 Hz, 1H), 7.14 (d, *J*= 9.8 Hz, 1H), 7.00 (d, *J*= 8.1 Hz, 1H), 6.91 (t, *J*= 7.5 Hz, 1H). ^{13}C NMR (101 MHz, DMSO-d_6) 159.00, 156.05, 145.90, 144.45, 143.66, 135.15, 131.54, 130.10, 130.05, 126.66, 126.50, 121.84, 119.89, 116.95, 130.05, 126.66, 126.50, 121.84, 119.89, 116.95. HRMS (ESI, *m/z*): calculated for $C_{16}H_{13}N_3O_4S$ $[M+H]^+$ 344.0700; found 344.0696.

4-(5-Methyl-6-oxo-3-(pyridin-3-yl)pyridazin-1(6H)-yl)benzenesulfonamide (**6c**)

Yield 154 mg (45 %). Light brown solid, m.p. 128-129 °C. ^{1}H NMR (400 MHz, DMSO-d_6) δ ppm 9.87 (s, 1H), 9.02 (s, 1H), 8.53 (s, 1H), 8.17 (s, 1H), 7.70 (s, 2H), 7.38 (s, 3H), 7.11 (s, 2H), 2.33 (s, 3H). ^{13}C NMR (101 MHz, DMSO-d_6) δ ppm 149.06, 148.75, 147.17, 141.29, 134.83, 134.49, 133.21, 127.74, 123.88, 112.67, 13.39. HRMS (ESI, *m/z*): calculated for $C_{16}H_{14}N_4O_3S$ $[M+H]^+$ 342.0787; found 342.0789.

4-(6-Oxo-3-(pyridin-4-yl)pyridazin-1(6H)-yl)benzenesulfonamide (**6d**)

Yield 283 mg (86 %). Orange solid, m.p. 282-283°C. ^{1}H NMR (400 MHz, DMSO-d_6) δ ppm 8.72 (dd, *J*= 4.6, 1.5 Hz, 2H), 8.25 (d, *J*= 9.8 Hz, 1H), 8.02 – 7.96 (m, 2H), 7.96 – 7.89 (m, 4H), 7.51 (s, 2H), 7.30 (d, *J*= 9.8 Hz, 1H). ^{13}C (101 MHz, DMSO-d_6) δ ppm 159.18, 150.94, 144.24,

144.00, 142.89, 141.62, 131.89, 131.41, 126.74, 126.61, 120.65. HRMS (ESI, *m/z*): calculated for $C_{15}H_{12}N_4O_3S$ $[M+H]^+$ 329.0703; found 329.0696.

4-(3-Methyl-6-oxo-5,6-dihydropyridazin-1(4H)-yl)benzenesulfonamide (**7a**)

Yield 147 mg (55 %). white crystal, m.p. 145-147 °C. ^{1}H NMR (400 MHz, DMSO-d_6) δ ppm ppm 8.28 (d, *J*= 8.4 Hz, 2H), 8.04 (d, *J*= 8.4 Hz, 2H), 7.60 (s, 2H), 3.17 (m, 1H), 1.33 (d, *J*= 6.9 Hz, 6H). ^{13}C NMR (101 MHz, DMSO-d_6) δ ppm 165.96, 156.97, 144.12, 141.26, 126.31, 124.55, 27.75, 26.14, 23.34. HRMS (ESI, *m/z*): calculated for $C_{11}H_{14}N_3O_3S$ $[M+H]^+$ 268.0751; found 268.0754.

4-(6-Oxo-3-phenyl-5,6-dihydropyridazin-1(4H)-yl)benzenesulfonamide (**7b**)

Yield 221 mg (67 %). White solid, m.p. 254-255 °C. ^{1}H NMR (400 MHz, DMSO-d_6) δ ppm 7.93 – 7.84 (m, 4H), 7.81 (d, *J*= 8.5 Hz, 2H), 7.52 – 7.45 (m, 3H), 7.39 (s, 2H), 3.17 (t, *J*= 8.0 Hz, 2H), 2.78 (t, *J*= 8.0 Hz, 2H). ^{13}C NMR (101 MHz, DMSO-d_6) δ ppm 166.17, 153.38, 144.29, 141.58, 135.75, 130.50, 129.10, 126.71, 126.44, 124.84, 27.93, 22.77. HRMS (ESI, *m/z*): calculated for $C_{16}H_{15}N_3O_3S$ $[M+H]^+$ 330.0907; found 330.0903.

4-(3-(4-Methoxyphenyl)-6-oxo-5,6-dihydropyridazin-1(4H)-yl)benzenesulfonamide (**7c**)

Yield 238 mg (66 %). White solid, m.p. 198-199 °C. ^{1}H NMR (400 MHz, DMSO-d_6) δ ppm 7.84 (m, 6H), 7.37 (s, 2H), 7.03 (d, *J*= 8.8 Hz, 2H), 3.82 (s, 3H), 3.13 (t, *J*= 8.0 Hz, 2H), 2.75 (t, *J*= 8.0 Hz, 2H). ^{13}C NMR (101 MHz, DMSO-d_6) δ ppm 166.19, 161.27, 153.22, 144.36, 141.42, 128.38, 128.09, 126.40, 124.71, 114.48, 55.80, 28.04, 22.63. HRMS (ESI, *m/z*): calculated for $C_{17}H_{17}N_3O_4S$ $[M+H]^+$ 360.1013; found 360.1014.

4-(3-(3,4-Dichlorophenyl)-6-oxo-5,6-dihydropyridazin-1(4H)-yl)benzenesulfonamide (**7d**)

Yield 194 mg (94 %). White solid, m.p. 267-268 °C. ^{1}H NMR (400 MHz, DMSO-d_6) δ ppm 8.06 (d, *J*= 2.1 Hz, 1H), 7.91 – 7.87 (m, 2H), 7.85 (dd, *J*= 8.5, 2.1 Hz, 1H), 7.80 – 7.75 (m, 2H), 7.74 (d, *J*= 8.5 Hz, 1H), 7.38 (s, 2H), 3.18 (t, *J*= 8.1 Hz, 2H), 2.79 (t, *J*= 8.1 Hz, 2H). ^{13}C NMR (101 MHz, DMSO-d_6) δ ppm 165.99, 151.14, 144.08, 141.82, 136.43, 132.98, 132.06, 131.28, 128.47, 126.87, 126.48, 125.08, 27.66, 22.66. HRMS (ESI, *m/z*): calculated for $C_{16}H_{13}Cl_2N_3O_3S$ $[M+H]^+$ 398.0128; found 398.0123.

4-(4,5-Dichloro-6-oxopyridazin-1(6H)-yl)benzenesulfonamide (**8a**)

Yield 269 mg (96 %). White solid, m.p. 258-259 °C. ^{1}H NMR (400 MHz, DMSO-d_6) δ ppm 8.39 (s, 1H), 7.98 (d, *J*= 8.5 Hz, 2H), 7.79 (d, *J*= 8.5 Hz, 2H), 7.50 (s, 2H). ^{13}C NMR (101 MHz,

DMSO-d_6) δ ppm 156.10, 144.43, 143.72, 137.38, 136.58, 134.58, 126.83, 126.77. HRMS (ESI, *m/z*): calculated for $C_{10}H_7Cl_2N_3O_3S$ [M+H]+ 319.9658; found 319.9654.

4-(1-Oxophthalazin-2(1H)-yl)benzenesulfonamide (**9a**)

Yield 263 mg (87 %). White solid, m.p. 247-248 °C. ^{1}H NMR (400 MHz, DMSO-d_6) δ ppm 8.63 (s, 1H), 8.35 (d, *J*= 7.8 Hz, 1H), 8.02 (d, *J*= 6.2 Hz, 2H), 7.95 (m, 3H), 7.87 (d, *J*= 8.6 Hz, 2H), 7.48 (s, 2H). ^{13}C NMR (101 MHz, DMSO-d_6) δ ppm 158.85, 144.72, 143.25, 139.87, 134.67, 133.05, 129.67, 128.05, 127.64, 126.77, 126.68, 126.60. HRMS (ESI, *m/z*): calculated for $C_{13}H_{11}N_4O_3S$ $[M+H]^+$ 303.0546; found 303.0531.

4-(7,8-Dimethoxy-1-oxophthalazin-2(1H)-yl)benzenesulfonamide (**9b**)

Yield 326 mg (90 %). White solid, m.p. 263-264 °C. ^{1}H NMR (400 MHz, DMSO-d_6) δ ppm 8.40 (s, 1H), 7.94 (d, *J*= 8.3 Hz, 2H), 7.81 (d, *J*= 8.3 Hz, 2H), 7.76 (s, 2H), 7.47 (s, 2H), 3.97 (s, 3H), 3.81 (s, 3H). ^{13}C NMR (101 MHz, DMSO-d_6) δ ppm 156.94, 156.14, 148.37, 145.14, 142.95, 139.31, 126.88, 126.47, 124.62, 124.46, 121.96, 119.90, 61.57, 56.92. HRMS (ESI, *m/z*): calculated for $C_{16}H_{15}N_3O_5S$ $[M+H]^+$ 362.0805; found 362.0819.

4-(4-Methyl-1-oxophthalazin-2(1H)-yl)benzenesulfonamide (**9c**)

Yield 243 mg (77 %). White solid, m.p. 257-258 °C. ^{1}H NMR (400 MHz, DMSO-d_6) δ ppm 8.37 (d, *J*= 7.8 Hz, 1H), 8.05 – 8.00 (m, 2H), 7.98 – 7.91 (m, 3H), 7.90 – 7.85 (m, 2H), 7.46 (s, 2H), 2.62 (s, 3H). ^{13}C NMR (101 MHz, DMSO-d_6) δ ppm 158.74, 145.34, 144.74, 143.06, 134.52, 132.73, 129.64, 127.88, 127.16, 126.57, 126.43, 19.16. HRMS (ESI, *m/z*): calculated for $C_{15}H_{14}N_3O_3S$ $[M+H]^+$ 316.0750; found 316.0762.

General Procedure (GP2) for the synthesis of compounds 8c-f, 8i-h

A mixture of 4-(4,5-dichloro-6-oxopyridazin-1(6H)-yl)benzenesulfonamide (1 mmol), triethylamine (0.15 ml, 1,1 mmol) and 1,05 mmol the appropriated amine in ethanol (15-25 ml) was heated under reflux for 24 hours. After cooling the precipitated solids were collected, washed with water, ethanol and dried to afford the title compound without any additional purification.

4-(5-Chloro-4-(4-ethylpiperazin-1-yl)-6-oxopyridazin-1(6H)-yl)benzenesulfonamide (**8c**)

Yield 490 mg (79 %). White solid, m.p. 261-261,5°C. ^{1}H NMR (400 MHz, DMSO-d_6) δ ppm 8.15 (s, 1H), 7.93 (d, *J*= 8.7 Hz, 2H), 7.75 (d, *J*= 8.7 Hz, 2H), 7.46 (s, 2H), 3.56 – 3.47 (t, *J*= 4.9 Hz, 4H), 2.39 (q, *J*= 7.2 Hz, 2H), 1.04 (t, *J*= 7.2 Hz, 3H). ^{13}C NMR (101 MHz, DMSO-d_6) δ

ppm 157.52, 147.63, 144.24, 143.56, 133.66, 126.63, 126.34, 113.62, 52.81, 51.97, 49.00, 12.29. HRMS (ESI, *m/z*): calculated for $C_{16}H_{20}ClN_5O_3S$ $[M+H]^+$ 398.1048; found 398.1049.

4-(4-(Azepan-1-yl)-5-chloro-6-oxopyridazin-1(6H)-yl)benzenesulfonamide (**8d**)

Yield 353 mg (92 %). White solid, m.p. 207-208 °C. ^{1}H NMR (400 MHz, DMSO-d_6) δ ppm 8.10 (s, 1H), 7.92 (d, *J*= 8.6 Hz, 2H), 7.76 (d, *J*= 8.6 Hz, 2H), 7.45 (s, 2H), 3.78 (t, *J*= 5.9 Hz, 4H), 1.79 (s, 4H), 1.57 (s, 4H). ^{13}C NMR (101 MHz, DMSO-d_6) δ ppm 157.61, 146.01, 144.33, 143.23, 132.11, 126.54, 126.08, 106.58, 52.10, 28.76, 26.50. HRMS (ESI, *m/z*): calculated for $C_{16}H_{19}ClN_4O_3S$ $[M+H]^+$ 383.0939; found 383.0937.

4-(5-Chloro-4-morpholino-6-oxopyridazin-1(6H)-yl)benzenesulfonamide (**8e**)

Yield 315 mg (85 %). White solid, m.p. 255-256 °C. ^{1}H NMR (400 MHz, DMSO-d_6) δ ppm 8.16 (s, 1H), 7.93 (d, *J*= 8.7 Hz, 2H), 7.76 (d, *J*= 8.7 Hz, 2H), 7.46 (s, 2H), 3.79 – 3.69 (m, 4H), 3.59 – 3.47 (m, 4H). ^{13}C NMR (101 MHz, DMSO-d_6) δ ppm 157.50, 147.60, 144.21, 143.61, 133.59, 126.65, 126.35, 114.22, 66.62, 49.35. HRMS (ESI, *m/z*): calculated for $C_{14}H_{15}ClN_4O_4S$ $[M+H]^+$ 371.0575; found 371.0562.

4-(5-Chloro-4-(3,4-dihydroisoquinolin-2(1H)-yl)-6-oxopyridazin-1(6H)-yl)benzenesulfonamide (**8f**)

Yield 190 mg (49 %). White solid, m.p. 283-284 °C. ^{1}H NMR (400 MHz, DMSO-d_6) δ ppm 8.23 (s, 1H), 7.94 (d, *J*= 8.6 Hz, 2H), 7.77 (d, *J*= 8.6 Hz, 2H), 7.47 (s, 2H), 7.22 (s, 4H), 4.76 (s, 2H), 3.81 (s, 2H), 3.01 (s, 2H). ^{13}C NMR NMR (101 MHz, DMSO-d_6) δ ppm 157.58, 147.64, 144.27, 143.53, 134.57, 133.72, 133.19, 129.20, 127.14, 126.74, 126.64, 126.61, 126.31, 112.51, 50.88, 47.34, 28.99. HRMS (ESI, *m/z*): calculated for $C_{19}H_{18}ClN_4O_3S$ $[M+H]^+$ 417.0783; found 417.0776.

4-(5-Chloro-6-oxo-4-(4-(pyridin-2-yl)piperazin-1-yl)pyridazin-1(6H)-yl)benzenesulfonamide (**8i**)

Yield 340 mg (81 %). Beige solid, m.p. 302-304°C. ^{1}H NMR (400 MHz, DMSO-d_6) δ ppm 8.18 (d, *J*= 15.0 Hz, 2H), 7.95 (d, *J*= 7.5 Hz, 2H), 7.78 (d, *J*= 7.4 Hz, 2H), 7.53 (d, *J*= 41.2 Hz, 3H), 6.89 (d, *J*= 7.9 Hz, 1H), 6.70 (s, 1H), 3.66 (s, 8H). ^{13}C NMR (101 MHz, DMSO-d_6) δ ppm 159.18, 157.53, 148.08, 147.69, 144.24, 143.58, 138.14, 133.66, 126.66, 126.33, 113.87, 107.74, 48.64, 45.19. HRMS (ESI, *m/z*): calculated for $C_{19}H_{20}ClN_6O_3S$ $[M+H]^+$ 447.1001; found 447.1015.

4-(4-(Benzylamino)-5-chloro-6-oxopyridazin-1(6H)-yl)benzenesulfonamide (**8g**)

Yield 207 mg (53 %). White solid, m.p. 225-226 °C. $_1$H NMR (400 MHz, DMSO-d_6) δ ppm 8.01 (s, 1H), 7.89 (d, *J*= 8.5 Hz, 2H), 7.72 (d, *J*= 8.5 Hz, 2H), 7.66 (t, *J*= 6.4 Hz, 1H), 7.44 (s, 2H), 7.38 (d, *J*= 4.3 Hz, 4H), 7.29 (m, 1H), 4.67 (d, *J*= 6.4 Hz, 2H). ^{13}C NMR (101 MHz, DMSO-d_6) δ ppm 156.71, 144.89, 144.33, 143.30, 139.42, 129.12, 129.00, 127.69, 127.32, 126.49, 126.33, 105.34, 45.69. HRMS (ESI, *m/z*): calculated for $C_{17}H_{15}ClN_4O_3S$ $[M+H]_+$ 391.0626; found 391.0619.

4-(5-Chloro-4-((3-morpholinopropyl)amino)-6-oxopyridazin-1(6H)-yl)benzenesulfonamide (**8h**)

Yield 294 mg (69 %). White solid, m.p. 196 -197 °C. ^{1}H NMR (400 MHz, DMSO-d_6) δ ppm 8.18 (s, 1H), 7.91 (d, *J*= 8.0 Hz, 2H), 7.74 (d, *J*= 7.9 Hz, 2H), 7.45 (s, 2H), 7.14 (s, 1H), 3.69 – 3.42 (m, 6H), 2.37 (s, 6H), 1.75 (s, 2H). ^{13}C NMR (101 MHz, DMSO-d_6) δ ppm 156.69, 145.02, 144.44, 143.22, 129.21, 126.52, 126.27, 104.36, 66.55, 56.30, 53.77, 41.74, 26.20. HRMS (ESI, *m/z*): calculated for $C_{17}H_{22}ClN_5O_4S$ $[M+H]^+$ 428.1154; found 428.1159.

General procedure 3 (GP3) of hydrogenation of 8a and 8c-i

The chloro compound (**8a** or **8c-i**) (1 mmol) was suspended in 20 mL of methanol with the addition of (2,1 or 1,1 mmol respectively) of triethylamine. After the mixture was purged with inert atmosphere, 5 mg of 10 % palladium on carbon catalyst (2-5 % by weight of **8a** or **8c-i**) was added, and the mixture was treated with hydrogen gas at 5 bar in a Parr hydrogenation apparatus for 16 h at 50 °C. The hot mixture was filtered through a Celite pad, and the pad was washed with 30 mL of boiling methanol. The filtrates were combined and evaporated in vacuo to dryness at 50 °C. The residue was triturated with water and filtered to yield of crude product. Recrystallization of a small sample from ethanol yielded an analytical sample.

4-(6-Oxopyridazin-1(6H)-yl)benzenesulfonamide (**8a**)

Yield 199 mg (79 %). white solid, m.p. 170-172 °C. ^{1}H NMR (400 MHz, DMSO-d_6) δ ppm 8.20 – 7.70 (m, 5H), 7.48 (s, 3H), 7.12 (s, 1H). ^{13}C NMR (101 MHz, DMSO-d_6) δ ppm 159.74, 144.28, 143.75, 138.51, 133.12, 131.35, 126.66, 126.46. HRMS (ESI, *m/z*): calculated for $C_{10}H_9N_3O_3S$ $[M+H]^+$ 252.0437; found 252.0449.

4-(4-(4-Ethylpiperazin-1-yl)-6-oxopyridazin-1(6H)-yl)benzenesulfonamide (**8c**)

Yield 233 mg (64 %). Beige solid, m.p. 221-222 °C. ^{1}H NMR (400 MHz, DMSO-d_6) δ ppm 8.24 (d, *J*= 2.7 Hz, 1H), 7.88 (d, *J*= 8.7 Hz, 2H), 7.75 (d, *J*= 8.7 Hz, 2H), 7.41 (s, 2H), 5.93 (d, *J*= 2.6 Hz, 1H), 3.56 – 3.38 (m, 4H), 2.48 – 2.41 (m, 4H), 2.37 (q, *J*= 7.2 Hz, 2H), 1.03 (t, *J*= 12.9, 5.8 Hz, 3H). ^{13}C NMR (126 MHz, DMSO-d_6) δ ppm 160.36, 149.95, 144.37, 142.78,

131.76, 126.42, 125.82, 100.02, 52.13, 51.92, 46.14, 12.36. HRMS (ESI, *m/z*): calculated for $C_{16}H_{21}N_5O_3S$ $[M+H]^+$ 364.1438; found 364.1444.

4-(4-(Azepan-1-yl)-6-oxopyridazin-1(6H)-yl)benzenesulfonamide (**8k**)

Yield 272 mg (78 %). White solid, m.p. 199-200 °C. ^{1}H NMR (400 MHz, DMSO-d_6) δ ppm 8.11 (d, *J*= 1.7 Hz, 1H), 7.89 (d, *J*= 8.4 Hz, 2H), 7.77 (d, *J*= 8.4 Hz, 2H), 7.42 (s, 2H), 5.71 (d, *J*= 1.5 Hz, 1H), 3.55 (s, 4H), 1.73 (s, 4H), 1.52 (s, 4H). ^{13}C NMR (101 MHz, DMSO-d_6) δ ppm 160.36, 148.52, 144.53, 142.56, 130.74, 126.36, 125.71, 96.37, 49.34, 26.49. HRMS (ESI, *m/z*): calculated for $C_{16}H_{20}N_4O_3S$ $[M+H]^+$ 349.1329; found 349.1328.

4-(4-Morpholino-6-oxopyridazin-1(6H)-yl)benzenesulfonamide (**8l**)

Yield 299 mg (89 %). White solid, m.p. 193-194°C. ^{1}H NMR (400 MHz, DMSO-d_6) δ ppm 8.24 (s, 1H), 7.84 (dd, *J*= 53.1, 8.4 Hz, 4H), 7.43 (s, 2H), 5.97 (s, 1H), 3.72 (s, 4H), 3.42 (s, 4H). ^{13}C (101 MHz, DMSO-d_6) δ ppm 160.35, 150.14, 144.33, 142.83, 131.59, 126.44, 125.83, 100.29, 65.96, 46.25. HRMS (ESI, *m/z*): calculated for $C_{14}H_{17}N_4O_4S$ $[M+H]^+$ 337.0965; found 337.0958.

4.3. Carbonic anhydrase inhibition assay

An Applied Photophysics stopped-flow instrument has been used for assaying the CA catalyzed CO_2 hydration activity [36]. Phenol red (at a concentration of 0.2 mM) has been used as indicator, working at the absorbance maximum of 557 nm, with 20 mM Tris (pH 8.3) as buffer, and 20 mM Na_2SO_4 (for maintaining constant the ionic strength), following the initial rates of the CA-catalyzed CO_2 hydration reaction for a period of 10–100 s. The CO_2 concentrations ranged from 1.7 to 17 mM for the determination of the kinetic parameters and inhibition constants. For each inhibitor at least six traces of the initial 5–10% of the reaction have been used for determining the initial velocity. The uncatalyzed rates were determined in the same manner and subtracted from the total observed rates. Stock solutions of inhibitor (0.1 mM) were prepared in distilled-deionized water and dilutions up to 0.005 nM were done thereafter with the assay buffer. Inhibitor and enzyme solutions were preincubated together for 15 min at room temperature prior to assay, in order to allow for the formation of the E-I complex. The inhibition constants were obtained by non-linear least-squares methods using PRISM 3 and the Cheng-Prusoff equation, as reported earlier, and represent the mean from at least three different determinations. All CA isoforms were recombinant ones obtained in-house [37-40].

4.4. Cell viability assay

Human cell lines were maintained at 37°C in humidified atmosphere containing air and 5% CO_2 as previously described [41]. Retinal pigment epithelial cells ARPE-19 were obtained from

American Type Culture Collection (ATCC, Manassas, VA, USA). Human melanoma cell line SK-MEL-2 were obtained from BioloT (Saint Petersburg, Russian Federation). Pancreas ductal adenocarcinoma cells PANC-1 were obtained from Russian collection cell cultures at the Institute of Cytology RAS (Saint Petersburg, Russian Federation). Cell line were grown in Dulbeccos Modified Eagle's Medium-F12 (BioloT) containing 10% (v/v) heat-inactivated fetal calf serum (FCS, HyClone Laboratories, UT, USA), 1% L-glutamine, 1% sodium pyruvate, 50 U/mL penicillin, and 50 μg/mL streptomycin (BioloT). Cytotoxicity of carbonic anhydrase inhibitors was evaluated using a routine colorimetric method with tetrazolium dye – 3-(4,5-dimethylthiazol-2-yl)-2,5-diphenyltetrazolium bromide (MTT). The cell lines were incubated for 48 h under normoxia and in the presence of the hypoxia-mimicking agent 50 μM Co^{2+} with medium containing different concentrations of carbonic anhydrase inhibitors. Following treatment, Dulbeccos Modified Eagle's Medium-F12 (100 μL/ well) and 20 μL of a 2.5 mg/mL MTT solution were added and cells were incubated for 1 h at 37 °C. The used cell density was 5 × 10^3 cells/200 μL/well in 96-well microtiter plates. After aspiration of the supernatants, the MTT-formazan crystals formed by metabolically active cells were dissolved in dimethyl sulfoxide (100 μL/well) and absorbance was measured at 540 nm and 690 nm in Varioskan LUX™ Multimode Microplate Reader (Thermo Scientific, USA). Values measured at 540 nm were subtracted for background correction at 690 nm, and the data were plotted as a percent of control untreated samples.

4.5. Molecular modeling studies

The crystal structures of *h*CA II (PDB code 2AW1) and *h*CA IX (PDB code 3IAI) were taken from the Protein Data Bank [42]. Molecular docking calculations were performed with AUTODOCK 4.2 [43] using the improved force field [44]. Autodock Tools were employed for identifying the torsion angles in the ligand, add the solvent model and assign the Kollman atomic charges to the protein. Ligand charges were calculated with the Gasteiger method. A grid spacing of 0.375 Å and a distance-dependent function of the dielectric constant were used for the energetic map calculations. The ligands were subjected to a robust docking procedure already used in virtual screening and pose prediction studies [45-46]. Each docked compound was subjected to 200 runs of the AUTODOCK search using the Lamarckian Genetic Algorithm performing 10 000 000 steps of energy evaluation. The number of individuals in the initial population was set to 500 and a maximum of 10 000 000 generations were simulated during each docking run. All other settings were left as their defaults and the best docked conformations were taken into account. The selected docking poses were then refined through energy minimization in explicit water environment [47]. The ligand-protein complexes were minimized employing

Amber 16 software [48] with ff14SB force field. The complexes were placed in a rectangular parallelepiped water box, using the TIP3P explicit solvent model for water, and were solvated with a 15 Å water cap. Sodium ions were added as counter ions to neutralize the system. Two minimization stages consisting of 5000 steps of steepest descent followed by conjugate gradient, until a convergence of 0.05 kcal/Å mol, were then performed. In the first one, the protein was kept rigid with a position restraint of 100 kcal/mol·$Å^2$ to uniquely minimize the positions of the water molecules. In the second stage, the entire system was energy minimized by applying a harmonic potential of 10 kcal/mol·$Å^2$ only to the protein α carbons.

Acknowledgements

This research was supported by the Russian Federation Government Megagrant 14.W03.031.0025. We are grateful to the Centre for Chemical Analysis and Materials Research of Saint Petersburg State University Research Park for the high-resolution mass-spectrometry data.

A. Supplementary material

Supplementary data associated with this article can be found, in the online version, at http://dx.doi.org/xxx.

References

[1] C. T. Supuran, Structure and function of carbonic anhydrases. Biochem. J. 473 (2016) 2023–2032.

[2] V. Alterio, A. Di Fiore, K. D'Ambrosio, C.T. Supuran, D. De Simone, Multiple Binding Modes of Inhibitors to Carbonic Anhydrases: How to Design Specific Drugs Targeting 15 Different Isoforms?, Chem. Rev. 112 (2012) 4421-4468.

[3] C.T. Supuran, Carbonic anhydrase inhibitors and activators for novel therapeutic applications, Future Med. Chem. 3 (2011) 1165-1180.

[4] C.T. Supuran, C. Capasso, The η-class carbonic anhydrases as drug targets for antimalarial agents, Expert Opin. Ther. Targets. 19 (2015) 551–563.

[5] C.T. Supuran, Diuretics: from classical carbonic anhydrase inhibitors to novel applications of the sulfonamides, Curr. Pharm. Des. 14 (2008) 641−648.

[6] C.T. Supuran, A. Scozzafava, F. Mincione, The development of topically acting carbonic anhydrase inhibitors as antiglaucoma agents, Curr. Pharm. Des. 14 (2008) 649−654.

[7] C.T. Supuran, Carbonic anhydrases: novel therapeutic applications for inhibitors and activators, Nat. Rev. Drug Discov., 7 (2008) 168-181.

[8] M. Krasavin, M. Korsakov, Z. Zvonaryova, E. Semyonychev, T. Tuccinardi, S. Kalinin, M. Tanç, C.T. Supuran, Human carbonic anhydrase inhibitory profile of mono- and bis-

sulfonamides synthesized via a direct sulfochlorination of 3-and 4-(hetero)arylisoxazol-5-amine scaffolds, Bioorg. Med. Chem. 25 (2017) 1914-1925.

[9] C.T. Supuran, S. Kalinin, M. Tanç, P. Sarnpitak, P. Mujumdar, S.-A. Poulsen, M. Krasavin, Isoform-selective inhibitory profile of 2-imidazoline-substituted benzenesulfonamides against a panel of human carbonic anhydrases, J. Enzyme Inhib. Med. Chem., 31 (Suppl. 1) (2016) 197-202.

[10] G. La Regina, A. Coluccia, V. Famiglini, S. Pelliccia, L. Monti, D. Vullo, E. Nuti, V. Alterio, G. De Simone, S. M. Monti, P. Pan, S. Parkkila, C.T. Supuran, A. Rossello, R. Silvestri, Discovery of 1,1′-Biphenyl-4-sulfonamides as a New Class of Potent and Selective Carbonic Anhydrase XIV Inhibitors, J. Med. Chem. 58 (2015) 8564-8572.

[11] J. Ivanova, F. Carta, D. Vullo, J. Leitans, A. Kazaks, K. Tars, R. Žalubovskis, C.T. Supuran, N-Substituted and ring opened saccharin derivatives selectively inhibit transmembrane, tumor-associated carbonic anhydrases IX and XII, Bioorg. Med. Chem. 25 (2017) 3583-3589.

[12] F. Carta, D. Vullo, S. M. Osman, Z. AlOthman, C. T. Supuran, Synthesis and Carbonic Anhydrase inhibition of a series of SLC-0111 analogs. Bioorg. Med. Chem. 25 (2017) 2569–2576.

[13] S. Singh, C. L. Lomelino, M. Y. Mboge, S. C. Frost, R. McKenna, Cancer Drug Development of Carbonic Anhydrase Inhibitors beyond the Active Site, Molecules 2018 (23) 1045.

[14] L. Schwartz, C. T. Supuran, K. O. Alfarouk, The Warburg effect and the hallmarks of cancer. Anticancer Agents Med. Chem. 17 (2017) 164–170.

[15] C. T. Supuran, Carbonic Anhydrase Inhibition and the Management of Hypoxic Tumors, Metabolites 48 (2017) 48.

[16] T. Yamaoka, M. Ohba, T. Ohmori, Molecular-Targeted Therapies for Epidermal Growth Factor Receptor and Its Resistance Mechanisms. Int. J. Mol. Sci. 18 (2017) E2420.

[17] A. Nocentini, C. T. Supuran, Carbonic anhydrase inhibitors as antitumor/antimetastatic agents: a patent review (2008-2018). Expert Opin. Ther. Pat. 28 (2018) 729-740.

[18] C.T. Supuran, How many carbonic anhydrase inhibition mechanisms exist?, J. Enzyme Inhib. Med. Chem. 31 (2016) 345–360.

[19] P.A. Boriack-Sjodin, S. Zeitlin, H.-H. Chen, L. Crenshaw, S. Gross, A. Dantanarayana, P. Delgado, J.A. May, T. Dean, D.W. Christianson, Structural analysis of inhibitor binding to human carbonic anhydrase II, Protein Sci. 7 (1998) 2483-2489.

[20] S. Kalinin, S. Kopylov, T. Tuccinardi, A. Sapegin, D. Dar'in, A. Angeli, C. T. Supuran, M. Krasavin, Lucky Switcheroo: Dramatic Potency and Selectivity Improvement of Imidazoline Inhibitors of Human Carbonic Anhydrase VII. ACS Med. Chem. Lett. 8 (2017) 1105-1109.

[21] M. Krasavin, M. Korsakov, M. Dorogov, T. Tuccinardi, N. Dedeoglu, C.T. Supuran, Probing the ‘bipolar nature of the carbonic anhydrase active site: Aromatic sulfonamides containing 1,3-oxazol-5-yl moiety as picomolar inhibitors of cytosolic CA I and CA II isoforms, Eur. J. Med. Chem. 101 (2015) 334-347.

[22] M. Krasavin, M. Korsakov, O. Ronzhina, T. Tuccinardi, S. Kalinin, M. Tanç, C. T. Supuran, Primary mono- and bis-sulfonamides obtained via regiospecific sulfochlorination of N-

arylpyrazoles: inhibition profile against a panel of human carbonic anhydrases. J. Enz. Inhib. Med. Chem. 32 (2017) 920-934.

[23] M. Krasavin, A. Shetnev, T. Sharonova, S. Baykov, T. Tuccinardi, K. Kalinin, A. Angeli, C. T. Supuran, Heterocyclic Periphery in the Design of Carbonic Anhydrase Inhibitors: 1,2,4-Oxadiazol-5-yl Benzenesulfonamides as Potent and Selective Inhibitors of Cytosolic hCA II and Membrane-Bound hCA IX Isoforms. Bioorg. Chem. 76 (2018) 88-97.

[24] R. Yaseen, D. Ekinci, M. Senturk, A. Dh. Hameed, S. Ovais, P. Rathore, M. Samim, K. Javed, C. T. Supuran, Pyridazinone substituted benzenesulfonamides as potent carbonic anhydrase inhibitors. Bioorg. Med. Chem. Lett. 26 (2016) 1337-1341.

[25] W. J. Coates, A. McKillop, One-Pot Preparation of 6-Substituted 3(2H)-Pyridazinones from Ketones. Synthesis (1993) 334-342.

[26] R. Bashir, S. Yaseen, S. Ovais, S. Ahmad, H. Hamid, M.S. Alam, M. Samim, K. Javed, Synthesis and biological evaluation of some novel sulfamoylphenyl-pyridazinone as anti-inflammatory agents (Part-II). J. Enzyme Inhib. Med. Chem. 27 (2012) 92-96.

[27] D. J. Katz, D. S. Wise, L. B. Townsend, Synthesis of pyridazine analogs of the naturally occurring nucleosides cytidine, uridine, deoxycytidine and deoxyuridine. J. Med. Chem. 25 (1982) 813–821.

[28] A. Purohit, H. Radeke, M. Azure, K. Hanson, T. Benetti, F. Su, P. Yalamanchili, M. Yu, M. Hayes, M. Guaraldi, M. Kagan, S. Robinson, D. Casebier, Synthesis and Biological Evaluation of Pyridazinone Analogues as Potential Cardiac Positron Emission Tomography Tracers. J. Med. Chem. 51 (2008) 2954–2970.

[29] P. C. Ting, R. Kuang, H. Wu, R. G. Aslanian, J. Cao, D. W. Kim, J. F. Lee, J. Schwerdt, G. Zhou, S. Wainhaus, T. A. Black, A. Cacciapuoti, P. M. McNicholas, Y. Xu, S. S. Walker, The synthesis and structure–activity relationship of pyridazinones as glucan synthase inhibitors. Bioorg. Med. Chem. Lett. 21 (2011) 1819-1822.

[30] A. Mateus, A. Treyer, C. Wegler, M. Karlgren, P. Matsson, P. Artursson, Intracellular drug bioavailability: a new predictor of system dependent drug disposition. Sci Rep. 7 (2017) 43047.

[31] A. Grandane, M. Tanc, L. Di Cesare Mannelli, F. Carta, C. Ghelardini, R. Žalubovskis, C. T. Supuran, Substituted sulfocoumarins are selective carbonic anhdydrase IX and XII inhibitors with significant cytotoxicity against colorectal cancer cells. J. Med. Chem. 58 (2015) 3975-3983.

[32] K. C. Dunn, A. E. Aotaki-Keen, F. R. Putkey, L. M. Hjelmeland, ARPE-19, a human retinal pigment epithelial cell line with differentiated properties. Exp. Eye Res. 62 (1996) 155-169.

[33] G. Rui, H. C. Silva, L. Carvalho, M. F. Botelho, A. Mota-Pinto, PaCa-2 and PANC-1 – pancreas ductal adenocarcinoma cell lines with neuroendocrine differentiation and somatostatin receptors. Sci. Rep. 6 (2016) 21648.

[34] M. S. Al Okail, Cobalt chloride, a chemical inducer of hypoxia-inducible factor-1a in U251 human glioblastoma cell line. J. Saudi Chem. Soc. 14 (2010) 197-201.

[35] A. Caunii, C. Oprean, M. Cristea, A. Ivan, C. Danciu, C. Tatu, V. Paunescu, D. Marti, G. Tzanakakis, D. A. Spandidos, A. Tsatsakis, R. Susan, C. Soica, S. Avram, C. Dehelean, Effects of ursolic and oleanolic on SK-MEL-2 melanoma cells: In vitro and in vivo assays. Int. J. Oncol. 51 (2017) 1651–1660.

[36] R.G. Khalifah, The carbon dioxide hydration activity of carbonic anhydrase I. Stop-flow kinetic studies on the native human isoenzymes B and C, J. Biol. Chem. 246 (1971) 2561-2573.

[37] A. Maresca, F. Carta, D. Vullo, C.T. Supuran, Dithiocarbamates strongly inhibit the β-class carbonic anhydrases from Mycobacterium tuberculosis, J. Enzyme Inhib. Med. Chem. 28 (2013) 407–411.

[38] D. Ekinci, N.I. Kurbanoglu, E. Salamci, M. Senturk, C.T. Supuran, Carbonic anhydrase inhibitors: inhibition of human and bovine isoenzymes by benzenesulphonamides, cyclitols and phenolic compounds, J. Enzyme Inhib. Med. Chem. 27 (2012) 845–848.

[39] D. Ekinci, L. Karagoz, D. Ekinci, M. Senturk, C.T. Supuran, Carbonic anhydrase inhibitors: in vitro inhibition of *α* isoforms (*h*CA I, *h*CA II, *b*CA III, *h*CA IV) by flavonoids, J. Enzyme Inhib. Med. Chem. 28 (2013) 283–288.

[40] C. Alp, A. Maresca, N.A. Alp, M.S. Gültekin, D. Ekinci, A. Scozzafava, C.T. Supuran, Secondary/tertiary benzenesulfonamides with inhibitory action against the cytosolic human carbonic anhydrase isoforms I and II, J. Enzyme Inhib. Med. Chem. 28 (2013) 294–298.

[41] A.V. Hubina, A.A. Pogodaev, V.V. Sharoyko, E.G. Vlakh, T.B. Tennikova, Self-assembled spin-labeled nanoparticles based on poly(amino acids). React. Funct. Polym. 100 (2016) 173-180.

[42] H.M. Berman, T. Battistuz, T.N. Bhat, W.F. Bluhm, P.E. Bourne, K. Burkhardt, Z. Feng, G.L. Gilliland, L. Iype, S. Jain, P. Fagan, J. Marvin, D. Padilla, V. Ravichandran, B. Schneider, N. Thanki, H. Weissig, J.D. Westbrook, C. Zardecki, The protein data bank, Acta Crystallogr. D: Biol. Crystallogr. 58 (2002) 899–907.

[43] G.M. Morris, R. Huey, W. Lindstrom, M.F. Sanner, R.K. Belew, D.S. Goodsell, A.J. Olson, AutoDock4 and AutoDockTools4: Automated docking with selective receptor flexibility, J. Comput. Chem. 30 (2009) 2785–2791.

[44] D. Santos-Martins, S. Forli, M.J. Ramos, A.J. Olson, AutoDock4(Zn): an improved AutoDock force field for small-molecule docking to zinc metalloproteins, J. Chem. Inf. Model. 54 (2014) 2371–2379.

[45] G. Poli, A. Gelain, F. Porta, A. Asai, A. Martinelli, T. Tuccinardi T. Identification of a new STAT3 dimerization inhibitor through a pharmacophore-based virtual screening approach. J. Enzyme. Inhib. Med. Chem. 31 (2016) 1011-1017.

[46] L. Milella, S. Milazzo, M. De Leo, M.B. Vera Saltos, I. Faraone, T. Tuccinardi, M. Lapillo, N. De Tommasi, A. Braca. α-Glucosidase and α-Amylase Inhibitors from Arcytophyllum thymifolium. J. Nat. Prod. 79 (2016) 2104-2112.

[47] M. Aghazadeh Tabrizi, P.G. Baraldi, E. Ruggiero, G. Saponaro, S. Baraldi, G. Poli, T. Tuccinardi, A. Ravani, F. Vincenzi, P.A. Borea, K. Varani. Synthesis and structure activity relationship investigation of triazolo[1,5-a]pyrimidines as CB2 cannabinoid receptor inverse agonists. Eur. J. Med. Chem. 113 (2016) 11-27.

[48] D.A. Case, J.T. Berryman, R.M. Betz, D.S. Cerutti, Darden, R.E. Duke, T.J. Giese, H. Gohlke, A.W. Goetz, N. Homeyer, S. Izadi, P. Janowski, J. Kaus, A. Kovalenko, T.S. Lee, S. LeGrand, P. Li, T. Luchko, R. Luo, B. Madej, K.M. Merz, G. Monard, P. Needham, H. Nguyen, H.T. Nguyen, I. Omelyan, A. Onufriev, D.R. Roe, A. Roitberg, R. Salomon-Ferrer, C.L. Simmerling, W. Smith, J. Swails, R.C. Walker, J. Wang, R.M. Wolf, X. Wu, D.M. York, P.A. Kollman, AMBER, Version 16, University of California, San Francisco, CA.

- A small set of pyridazine carbonic anhydrase inhibitors (CAIs) was reported earlier
- A larger set was designed which delivered potent inhibitors of CA IX isoform
- This membrane-bound isoform is considered a promising cancer target
- Two compounds showed potential to selectively kill cancer cells
- SAR findings have been rationalized by *in silico* docking experiments